LA-UR- 98-23

Title: ENDF/B-V AND ENDF/B-VI RESULTS FOR UO-2 LATTICE BENCHMARK PROBLEMS USING MCNP

CONF-981003--

Author(s): R. D. Mosteller

RECEIVED
MAY 28 1998
OSTI

Submitted to: Int'l Conf. on Physics of Nuclear Science & Technology, Islandia, Long Island, NY
October 5-8, 1998

MASTER

DISTRIBUTION OF THIS DOCUMENT IS UNLIMITED

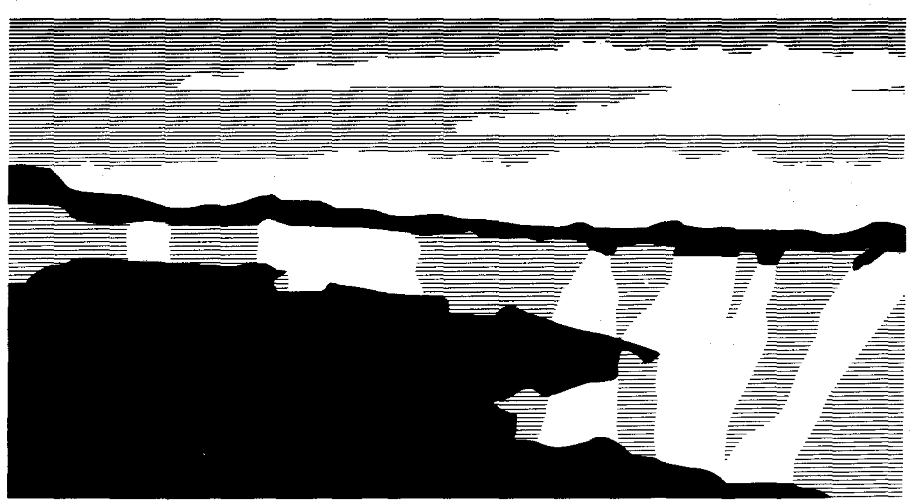

Los Alamos
NATIONAL LABORATORY

DISCLAIMER

Portions of this document may be illegible in electronic image products. Images are produced from the best available original document.

LA-UR- 98-23

ENDF/B-V AND ENDF/B-VI RESULTS FOR

UO_2 LATTICE BENCHMARK PROBLEMS

USING MCNP

Russell D. Mosteller

Advanced Nuclear Technology Group
Nonproliferation and International Security Division
Los Alamos National Laboratory

To Be Submitted for Presentation at the
International Conference on the Physics of Nuclear Science and Technology

Islandia, Long Island, NY October 5-8, 1998

ENDF/B-V AND ENDF/B-VI RESULTS FOR UO_2 LATTICE BENCHMARK PROBLEMS USING MCNP

Calculations for the ANS UO_2 lattice benchmark[1] have been performed with the MCNP Monte Carlo code[2] and its ENDF/B-V and ENDF/B-VI continuous-energy libraries. Similar calculations were performed previously[3] for the experiments upon which these benchmarks are based, using continuous-energy libraries derived from ENDF/B-V and from Release 2 of ENDF/B-VI (ENDF/B-VI.2). This study extends those calculations to the infinite-lattice configurations given in the benchmark specifications and also includes results from Release 3 of ENDF/B-VI (ENDF/B-VI.3) for both the core and infinite-lattice configurations.

For this set of benchmarks, the only significant difference between the ENDF/B-VI.2 and ENDF/B-VI.3 libraries is the cross-section behavior of ^{235}U. ENDF/B-VI.3 contains revised cross sections for ^{235}U below 900 eV,[4] although those changes principally affect the range below 110 eV.[5,6] In particular, relative to ENDF/B-VI.2, ENDF/B-VI.3 increases the epithermal capture-to-fission ratio for ^{235}U and slightly increases its thermal fission cross section.

Each MCNP case discussed herein was run with 4,000 particles per generation and 1,050 generations. The first 50 generations were excluded from the statistics, thereby producing 4,000,000 active histories for each case.

The values for k_{eff} for the core problems are reported in Table 1, along with the resulting differences from the benchmark value (1.0007 ± 0.0006). The corresponding pin power distributions in the central assembly are shown in Figures 1 and 2.

ENDF/B-V appears to underpredict k_{eff} slightly for these cases. However, it has been reported[7] that deficiencies in the MCNP ENDF/B-V library for ^{238}U produce a bias of approximately -.003 Δk in the calculated value of k_{eff} for thermal lattices with low-enriched UO_2 fuel. If that bias is applied to these results, ENDF/B-V produces excellent agreement with the benchmark value for k_{eff}: all three values for k_{eff} are within 2 standard deviations of the benchmark value, and the difference between the benchmark and calculated means is 0.0012 Δk or less.

The ENDF/B-VI results for k_{eff} are not as good as those from ENDF/B-V. The calculated values of k_{eff} are approximately half a percent too low, with the ENDF/B-VI.3 value slightly but consistently lower than the ENDF/B-VI.2 value.

The pin power distributions from the three libraries all are in good agreement with the measured values, with an RMS difference of approximately 2% between the measured and calculated sample means. The RMS differences between the calculated sample means are slightly smaller, ranging from 1.1% to 1.9%. However, it is likely that the size of these differences would decrease somewhat if additional Monte Carlo histories were run to reduce the calculated standard deviations.

The values for k_{eff} and the various spectral indices from the infinite-lattice calculations are reported in Table 2, and the corresponding pin power distributions are shown in Figures 3 and 4. Not surprisingly, the results from the infinite-lattice cases produce patterns that are similar to those observed for the core cases. For example, the RMS differences between the pin power distributions for the infinite-lattices cases are only 0.3% to 0.4%, which is comparable to the standard deviations in the pin powers. These results, in conjunction with those for the core problems, strongly suggest that all three libraries produce essentially the same power distributions for these benchmarks.

Nonetheless, there are subtle changes to the reactivity differences that reflect cross section differences between the libraries. In particular, the reactivity differences between the ENDF/B-V and ENDF/B-VI results decrease slightly relative to the core cases, which suggests that leakage from the core to the reflector is slightly higher for the ENDF/B-VI cases. Such behavior is consistent with differences in the ENDF/B-V and ENDF/B-VI cross sections for ^{16}O at high energies.

Differences in the spectral indices also reflect cross section differences between the libraries and thereby help to explain the observed reactivity differences. The values for ρ_{25} are consistent with the epithermal ^{235}U capture-to-fission ratio in the three libraries (i.e., ρ_{25} is lowest for ENDF/B-VI.2 and highest for ENDF/B-VI.3). The results from both ENDF/B-VI libraries for ρ_{28} and for the conversion ratio are higher than those from ENDF/B-V, and such behavior indicates higher neutron capture rates in ^{238}U (the ENDF/B-VI.3 values are slightly but consistently lower than their ENDF/B-VI.2 counterparts, reflecting the increased competition between ^{235}U and ^{238}U in the epithermal region). All three libraries produce essentially the same values for δ_{28} but the ENDF/B-VI values for δ_{25} are lower than those from the ENDF/B-V calculations. This combination suggests that reactivity differences between ENDF/B-VI and ENDF/B-V are due, at least in part, to increased fast capture in ^{238}U and decreased fast fission in ^{235}U.

Overall, ENDF/B-V produces significantly better agreement with the benchmark values for k_{eff} than do either of the ENDF/B-VI libraries. The pin power distributions, however, are essentially the same irrespective of the library. Finally, the spectral indices from the infinite-lattice cases are consistent with the known cross section behavior in the three libraries and help to explain the observed reactivity differences.

References

1. T. A. Parish, et al., "Summary of Results For the ANS Uranium Benchmark Problem," submitted for presentation at the International Conference on the Physics of Nuclear Science and Technology.

2. Judith A. Briesmeister, Ed., "MCNP—A General Monte Carlo N-Particle Transport Code, Version 4A," Los Alamos National Laboratory report LA-12625-M (November 1993).

3. Russell D. Mosteller, Stephanie C. Frankle, and Phillip G. Young, "Data Testing of ENDF/B-VI with MCNP: Critical Experiments, Thermal-Reactor Lattices, and Time-of-Flight Measurements," Jeffrey Lewins and Martin Becker, Eds., **Advances in Nuclear Science and Technology, Volume 24**, pp. 131-195, Plenum Press (1997).

4. C. R. Lubitz, "A Modification to ENDF/B-VI ^{235}U to Increase Epithermal Alpha and K_1," *Proceedings of the International Conference on Nuclear Data for Science and Technology*, CONF-940507 (May 1994).

5. A. C. Kahler, "Homogeneous Critical Monte Carlo Eigenvalue Calculations with Revised ENDF/B-VI Data Sets," *Trans. Am. Nucl. Soc.*, **72**, 384 (June 1995).

6. M. L. Williams, R. Q. Wright, and M. Asgari, "ENDF/B-VI Performance for Thermal Reactor Analysis," *Trans. Am. Nucl. Soc.*, **73**, 420 (October 1995).

7. F. Rahnema and H. N. M. Gheorghiu, "ENDF/B-VI Benchmark Calculations for the Doppler Coefficient of Reactivity," *Ann. Nucl. Energy*, **23**, No. 12, pp. 1011- 1019 (August 1996).

Table 1. MCNP Results for Core Configurations.

Core	k_{eff}			Δk		
	ENDF/B-V	ENDF/B-VI.2	ENDF/B-VI.3	ENDF/B-V	ENDF/B-VI.2	ENDF/B-VI.3
A	0.9981 ± 0.0003	0.9963 ± 0.0003	0.9956 ± 0.0003	-0.0026 ± 0.0007	-0.0044 ± 0.0007	-0.0051 ± 0.0007
B	0.9988 ± 0.0003	0.9964 ± 0.0003	0.9957 ± 0.0003	-0.0019 ± 0.0007	-0.0043 ± 0.0007	-0.0050 ± 0.0007
C	0.9965 ± 0.0003	0.9944 ± 0.0003	0.9940 ± 0.0003	-0.0042 ± 0.0007	-0.0063 ± 0.0007	-0.0067 ± 0.0007

Water Hole	1.107 ± 0.002 1.122 ± 0.013 1.124 ± 0.013 1.119 ± 0.013	1.026 ± 0.006 1.028 ± 0.012 1.049 ± 0.012 1.059 ± 0.012	1.000 ± 0.001 1.014 ± 0.012 1.025 ± 0.012 1.017 ± 0.011	1.025 ± 0.007 1.005 ± 0.012 1.019 ± 0.012 1.028 ± 0.012	1.026 ± 0.003 1.002 ± 0.011 1.040 ± 0.012 1.021 ± 0.012	0.980 ± 0.021 0.989 ± 0.011 1.008 ± 0.011 0.978 ± 0.011	0.983 ± 0.008 0.963 ± 0.011 0.966 ± 0.011 0.963 ± 0.011
	1.068 ± 0.002 1.080 ± 0.012 1.088 ± 0.012 1.072 ± 0.012	1.075 ± 0.000 1.096 ± 0.009 1.117 ± 0.010 1.107 ± 0.009	1.036 ± 0.007 1.049 ± 0.009 1.060 ± 0.009 1.051 ± 0.009	1.047 ± 0.004 1.045 ± 0.009 1.048 ± 0.009 1.047 ± 0.009	1.098 ± 0.006 1.074 ± 0.009 1.098 ± 0.009 1.070 ± 0.009	1.026 ± 0.023 1.018 ± 0.008 1.026 ± 0.009 1.013 ± 0.009	1.003 ± 0.031 0.969 ± 0.008 0.958 ± 0.008 0.969 ± 0.008
		Water Hole	1.116 ± 0.012 1.130 ± 0.009 1.139 ± 0.009 1.113 ± 0.009	1.118 ± 0.011 1.137 ± 0.009 1.117 ± 0.009 1.139 ± 0.009	Water Hole	1.070 ± 0.010 1.083 ± 0.009 1.070 ± 0.009 1.073 ± 0.009	0.961 ± 0.010 0.979 ± 0.008 0.990 ± 0.008 0.984 ± 0.008
			1.091 ± 0.009 1.071 ± 0.012 1.101 ± 0.012 1.097 ± 0.012	1.145 ± 0.008 1.152 ± 0.009 1.152 ± 0.009 1.148 ± 0.009	1.133 ± 0.010 1.128 ± 0.009 1.123 ± 0.009 1.135 ± 0.009	1.032 ± 0.026 1.019 ± 0.008 1.007 ± 0.008 1.030 ± 0.008	0.924 ± 0.006 0.987 ± 0.008 0.974 ± 0.008 0.972 ± 0.008
				Water Hole	1.109 ± 0.007 1.096 ± 0.009 1.087 ± 0.009 1.095 ± 0.009	1.007 ± 0.014 1.008 ± 0.008 0.974 ± 0.008 1.003 ± 0.009	0.974 ± 0.026 0.961 ± 0.008 0.949 ± 0.008 0.953 ± 0.008
					1.015 ± 0.002 1.010 ± 0.011 1.006 ± 0.012 1.019 ± 0.012	0.973 ± 0.023 0.980 ± 0.008 0.960 ± 0.008 0.976 ± 0.008	0.971 ± 0.012 0.955 ± 0.008 0.939 ± 0.008 0.944 ± 0.008
						0.970 ± 0.006 0.960 ± 0.012 0.952 ± 0.011 0.932 ± 0.011	0.950 ± 0.005 0.931 ± 0.008 0.934 ± 0.008 0.937 ± 0.008
						Measured ENDF/B-V ENDF/B-VI.2 ENDF/B-VI.3	0.920 ± 0.013 0.919 ± 0.011 0.934 ± 0.011 0.934 ± 0.011

RMS Differences
between Sample Means

ENDF/B-V:	0.020
ENDF/B-VI.2:	0.024
ENDF/B-VI.3	0.019

Figure 1. Pin Power Distribution in Central Assembly of Core B.

Water Hole	1.148 ± 0.007 1.152 ± 0.020 1.175 ± 0.020 1.144 ± 0.019	1.027 ± 0.004 1.050 ± 0.017 1.059 ± 0.017 1.048 ± 0.017	1.045 ± 0.006 1.039 ± 0.017 1.050 ± 0.017 1.021 ± 0.016	1.057 ± 0.006 1.021 ± 0.016 1.028 ± 0.016 1.034 ± 0.017	1.047 ± 0.005 1.066 ± 0.017 1.035 ± 0.017 1.009 ± 0.016	1.088 ± 0.004 1.072 ± 0.017 1.080 ± 0.017 1.106 ± 0.017	1.124 ± 0.016 1.124 ± 0.017 1.118 ± 0.017 1.114 ± 0.017
	1.036 ± 0.005 1.067 ± 0.018 1.102 ± 0.018 1.069 ± 0.018	0.945 ± 0.007 0.939 ± 0.012 0.965 ± 0.012 0.957 ± 0.012	1.001 ± 0.006 1.009 ± 0.012 0.998 ± 0.012 0.967 ± 0.012	0.982 ± 0.021 0.997 ± 0.012 0.991 ± 0.012 0.985 ± 0.012	0.962 ± 0.008 0.963 ± 0.011 0.962 ± 0.012 0.958 ± 0.012	1.070 ± 0.014 1.060 ± 0.012 1.063 ± 0.012 1.050 ± 0.012	1.105 ± 0.009 1.123 ± 0.013 1.104 ± 0.013 1.099 ± 0.009
		Pyrex Rod	0.901 ± 0.006 0.908 ± 0.011 0.891 ± 0.011 0.902 ± 0.011	0.900 ± 0.019 0.897 ± 0.011 0.900 ± 0.011 0.890 ± 0.011	Pyrex Rod	1.001 ± 0.021 0.990 ± 0.011 1.004 ± 0.012 1.005 ± 0.012	1.087 ± 0.007 1.094 ± 0.012 1.094 ± 0.012 1.097 ± 0.012
			0.914 ± 0.004 0.924 ± 0.016 0.927 ± 0.016 0.938 ± 0.016	0.854 ± 0.017 0.866 ± 0.011 0.893 ± 0.011 0.878 ± 0.011	0.933 ± 0.005 0.909 ± 0.011 0.915 ± 0.011 0.912 ± 0.011	1.049 ± 0.014 1.035 ± 0.012 1.056 ± 0.012 1.033 ± 0.012	1.088 ± 0.005 1.120 ± 0.012 1.094 ± 0.012 1.122 ± 0.012
				Pyrex Rod	0.970 ± 0.006 0.950 ± 0.012 0.959 ± 0.012 0.954 ± 0.011	1.097 ± 0.020 1.096 ± 0.012 1.106 ± 0.012 1.105 ± 0.012	1.138 ± 0.015 1.149 ± 0.013 1.135 ± 0.013 1.146 ± 0.013
					1.071 ± 0.006 1.050 ± 0.016 1.057 ± 0.016 1.087 ± 0.017	1.140 ± 0.014 1.133 ± 0.013 1.135 ± 0.013 1.145 ± 0.013	1.195 ± 0.006 1.164 ± 0.013 1.144 ± 0.013 1.173 ± 0.013
						1.164 ± 0.003 1.150 ± 0.018 1.157 ± 0.017 1.181 ± 0.018	1.199 ± 0.008 1.198 ± 0.013 1.171 ± 0.013 1.209 ± 0.013
						Measured ENDF/B-V ENDF/B-VI.2 ENDF/B-VI.3	1.206 ± 0.011 1.244 ± 0.019 1.215 ± 0.018 1.238 ± 0.018

RMS Differences
between Sample Means

ENDF/B-V: 0.016
ENDF/B-VI.2: 0.020
ENDF/B-VI.3: 0.019

Figure 2. Pin Power Distribution in Central Assembly of Core C.

Table 2. MCNP Results for Infinite-Lattice Configurations.

Configuration	Parameter	ENDF/B-V	ENDF/B-VI.2	ENDF/B-VI.3
A	k_∞	1.0582 ± 0.0003	1.0562 ± 0.0003	1.0560 ± 0.0003
	δ_{25}	0.1324 ± 0.0001	0.1309 ± 0.0001	0.1297 ± 0.0001
	δ_{28}	0.0647 ± 0.0001	0.0649 ± 0.0001	0.0649 ± 0.0001
	ρ_{25}	0.3475 ± 0.0003	0.3374 ± 0.0003	0.3619 ± 0.0004
	ρ_{28}	2.2774 ± 0.0023	2.2980 ± 0.0024	0.2923 ± 0.0024
	CR*	0.4676 ± 0.0003	0.4726 ± 0.0003	0.4710 ± 0.0004
B	k_∞	1.0486 ± 0.0003	1.0471 ± 0.0003	1.0466 ± 0.0003
	δ_{25}	0.1176 ± 0.0001	0.1163 ± 0.0001	0.1153 ± 0.0001
	δ_{28}	0.0600 ± 0.0001	0.0601 ± 0.0001	0.0601 ± 0.0001
	ρ_{25}	0.3089 ± 0.0003	0.2999 ± 0.0003	0.3211 ± 0.0003
	ρ_{28}	2.0282 ± 0.0021	2.0494 ± 0.0023	2.0448 ± 0.0023
	CR*	0.4380 ± 0.0003	0.4427 ± 0.0003	0.4414 ± 0.0003
C	k_∞	0.9860 ± 0.0003	0.9850 ± 0.0003	0.9842 ± 0.0003
	δ_{25}	0.1307 ± 0.0001	0.1293 ± 0.0001	0.1282 ± 0.0001
	δ_{28}	0.0656 ± 0.0001	0.0656 ± 0.0001	0.0658 ± 0.0001
	ρ_{25}	0.3442 ± 0.0004	0.3339 ± 0.0004	0.3585 ± 0.0004
	ρ_{28}	2.2729 ± 0.0025	2.2874 ± 0.0025	2.2859 ± 0.0025
	CR*	0.4670 ± 0.0004	0.4710 ± 0.0004	0.4700 ± 0.0004
	PAF**	0.1393 ± 0.0002	0.1387 ± 0.0002	0.1389 ± 0.0002

* Conversion Ratio
** Pyrex Absorption Fraction

Water Hole	1.051 ± 0.004 1.060 ± 0.004 1.054 ± 0.004	0.998 ± 0.003 0.998 ± 0.003 0.996 ± 0.003	0.977 ± 0.003 0.975 ± 0.003 0.972 ± 0.003	0.970 ± 0.003 0.971 ± 0.003 0.971 ± 0.003	0.979 ± 0.003 0.979 ± 0.003 0.978 ± 0.003	0.953 ± 0.003 0.961 ± 0.003 0.959 ± 0.003	0.946 ± 0.003 0.948 ± 0.003 0.944 ± 0.003
	1.020 ± 0.003 1.028 ± 0.003 1.022 ± 0.003	1.051 ± 0.002 1.049 ± 0.002 1.052 ± 0.002	1.003 ± 0.002 0.998 ± 0.002 0.998 ± 0.002	0.999 ± 0.002 0.998 ± 0.002 1.001 ± 0.002	1.040 ± 0.002 1.041 ± 0.002 1.040 ± 0.002	0.980 ± 0.002 0.983 ± 0.002 0.980 ± 0.002	0.945 ± 0.002 0.950 ± 0.002 0.951 ± 0.002
		Water Hole	1.069 ± 0.002 1.070 ± 0.002 1.065 ± 0.002	1.076 ± 0.002 1.072 ± 0.002 1.079 ± 0.002	Water Hole	1.035 ± 0.002 1.042 ± 0.002 1.038 ± 0.002	0.962 ± 0.002 0.962 ± 0.002 0.967 ± 0.002
			1.047 ± 0.003 1.048 ± 0.003 1.050 ± 0.003	1.090 ± 0.002 1.095 ± 0.002 1.094 ± 0.002	1.080 ± 0.002 1.081 ± 0.002 1.081 ± 0.002	0.992 ± 0.002 0.994 ± 0.002 0.993 ± 0.002	0.962 ± 0.002 0.962 ± 0.002 0.967 ± 0.002
				Water Hole	1.060 ± 0.002 1.053 ± 0.002 1.058 ± 0.002	0.974 ± 0.002 0.971 ± 0.002 0.969 ± 0.002	0.947 ± 0.002 0.950 ± 0.002 0.945 ± 0.002
					0.990 ± 0.003 0.987 ± 0.003 0.990 ± 0.003	0.952 ± 0.002 0.949 ± 0.002 0.954 ± 0.002	0.944 ± 0.002 0.941 ± 0.002 0.942 ± 0.002
						0.943 ± 0.003 0.939 ± 0.003 0.941 ± 0.003	0.938 ± 0.002 0.936 ± 0.002 0.934 ± 0.002
						ENDF/B-V ENDF/B-VI.2 ENDF/B-VI.3	0.939 ± 0.003 0.932 ± 0.003 0.937 ± 0.003

Figure 3. Assembly Pin Power Distribution for Infinite Lattice Configuration B.

Water Hole	1.135 ± 0.004 1.131 ± 0.004 1.137 ± 0.004	1.018 ± 0.003 1.015 ± 0.003 1.016 ± 0.003	1.007 ± 0.003 1.004 ± 0.003 1.009 ± 0.003	1.002 ± 0.003 1.001 ± 0.003 1.000 ± 0.003	0.999 ± 0.003 1.001 ± 0.003 1.003 ± 0.003	1.039 ± 0.003 1.036 ± 0.003 1.037 ± 0.003	1.067 ± 0.004 1.066 ± 0.004 1.059 ± 0.004
	1.037 ± 0.003 1.038 ± 0.003 1.037 ± 0.003	0.932 ± 0.002 0.932 ± 0.002 0.930 ± 0.002	0.968 ± 0.002 0.969 ± 0.002 0.968 ± 0.002	0.963 ± 0.002 0.963 ± 0.002 0.964 ± 0.002	0.932 ± 0.002 0.932 ± 0.002 0.930 ± 0.002	1.006 ± 0.002 1.010 ± 0.002 1.005 ± 0.002	1.056 ± 0.003 1.058 ± 0.003 1.054 ± 0.003
		Pyrex Rod	0.874 ± 0.002 0.874 ± 0.002 0.876 ± 0.002	0.868 ± 0.002 0.869 ± 0.002 0.870 ± 0.002	Pyrex Rod	0.948 ± 0.002 0.944 ± 0.002 0.943 ± 0.002	1.047 ± 0.002 1.049 ± 0.002 1.043 ± 0.002
			0.893 ± 0.003 0.895 ± 0.003 0.891 ± 0.003	0.849 ± 0.002 0.851 ± 0.002 0.848 ± 0.002	0.882 ± 0.002 0.883 ± 0.002 0.881 ± 0.002	1.007 ± 0.002 1.008 ± 0.002 1.006 ± 0.002	1.073 ± 0.003 1.063 ± 0.003 1.068 ± 0.003
				Pyrex Rod	0.925 ± 0.002 0.923 ± 0.002 0.924 ± 0.002	1.043 ± 0.002 1.046 ± 0.002 1.047 ± 0.002	1.086 ± 0.003 1.087 ± 0.003 1.089 ± 0.003
					1.022 ± 0.003 1.022 ± 0.003 1.020 ± 0.003	1.081 ± 0.002 1.086 ± 0.002 1.086 ± 0.002	1.105 ± 0.003 1.105 ± 0.003 1.113 ± 0.003
						1.113 ± 0.003 1.109 ± 0.003 1.117 ± 0.003	1.125 ± 0.003 1.128 ± 0.003 1.129 ± 0.003
						ENDF/B-V ENDF/B-VI.2 ENDF/B-VI.3	1.135 ± 0.004 1.137 ± 0.004 1.138 ± 0.004

Figure 4. Assembly Pin Power Distribution for Infinite Lattice Configuration C.

RMS Differences between Libraries

Case	ENDF/B-V vs ENDF/B-VI.2	ENDF/B-V vs ENDF/B-VI.3	ENDF/B-VI.2 vs ENDF/B-VI.3
Core B	0.016	0.011	0.015
Core C	0.016	0.017	0.018
Infinite Lattice B	0.004	0.003	0.004
Infinite Lattice C	0.003	0.003	0.003